Society For Biomaterials

Controlled-rate freezing to regulate the structure of collagen–glycosaminoglycan scaffolds in engineered skin substitutes

Christopher Lloyd,[1,2] John Besse,[2] Steven Boyce[1,2,3]

[1]University of Cincinnati, Surgery
[2]Shriners Hospitals for Children, Research
[3]University of Cincinnati, Biomedical, Chemical and Environmental Engineering

Received 17 January 2014; revised 18 June 2014; accepted 16 July 2014
Published online 00 Month 2014 in Wiley Online Library (wileyonlinelibrary.com). DOI: 10.1002/jbm.b.33253

Abstract: Controlled-rate freezing (CRF) of biopolymer scaffolds may increase reproducibility of microstructure compared with analog processes. Freezing of collagen–glycosaminoglycan (CG) scaffolds by CRF with liquid nitrogen at chamber cooling rates of −80, −40, −20, or −10°C/min, was compared with submersion in 95% ethanol at −55°C. Cooling rates of −80 or −40°C/min generated scaffolds with pore areas and pore fractions that were comparable to scaffolds frozen in ethanol. Test and control scaffolds were populated with human dermal fibroblasts and epidermal keratinocytes to generate engineered skin substitutes (ESS) and evaluated for surface hydration and mitochondrial metabolism. ESS with scaffolds frozen by CRF at −80 or −40°C/min were comparable with, or better than, ESS with control scaffolds ($p < 0.05$). These results demonstrate that fabrication of CG scaffolds by CRF offers advantages of digital programming, as well as greater reproducibility, safety, and simplicity than submersion in chilled ethanol without compromise of biological properties required for biomedical applications. © 2014 Wiley Periodicals, Inc. J Biomed Mater Res Part B: Appl Biomater 00B: 000–000, 2014.

Key Words: engineered skin, collagen scaffold, porosity, controlled-rate freezing, tissue engineering

How to cite this article: Lloyd C, Besse J, Boyce S. 2014. Controlled-rate freezing to regulate the structure of collagen–glycosaminoglycan scaffolds in engineered skin substitutes. J Biomed Mater Res Part B 2014: 00B: 000–000.

INTRODUCTION

Collagen type I from skin and tendon is highly conserved teleologically and has optimal compatibility as a biomaterial. For these reasons, collagen has served as the fundamental component in a wide variety of engineered tissues, including skin, bone, blood vessels, tracheae, and nerve [1–5]

Collagen can be processed into scaffolds that are fabricated with qualities to promote cellular attachment and morphogenesis of tissue substitutes for applications in regenerative medicine. Among the critical qualities for engineered tissues are biocompatibility, cellular adhesion, low hemostatic and inflammatory activities, and predictable structure and mechanical properties.[6] Chemical composition, pore size, and degradation rate may also be controlled to regulate how cells attach, proliferate, and differentiate after inoculation onto collagen-based scaffolds. Pore size can be optimized for cellular attachment, migration, and proliferation by several different methods including, but not limited to, lyophilization, electrospinning, or solvent casting.[4,7–9] Of these approaches, freeze-drying has been reported by numerous laboratories.[8,10–12] During freeze-drying, the pore size and structure of the dry scaffold results from nucleation and crystallization of ice in the aqueous homogenate. As the ice crystals form, solutes in the homogenate are excluded from the solvent and distributed into reticulations formed between adjacent ice crystals.[13] It is well understood that the size and distribution of pores in lyophilized collagen scaffolds results from the rate of freezing of water which regulates inversely the size of crystalline ice in the polymer homogenate.[10,11,14] Therefore, the faster the rate of freezing, the smaller the pore size in the scaffolds. By this process, instantaneous freezing generates vitreous ice, which has no crystalline structure[15,16] and results in formation of a film rather than a reticulated scaffold with a large pore volume.

Several laboratories have reported processes to control the random nature of ice nucleation to improve structural uniformity of lyophilized scaffolds. Previous studies from this laboratory demonstrated that collagen–glycosaminoglycan (CG) homogenates frozen in an isopropanol bath, chilled at incremental temperatures between −50 and −20°C generates CG scaffolds with increasing pore diameters.[11] Liquid

Correspondence to: S. Boyce; e-mail: steven.boyce@uc.edu
Contract grant sponsor: NIH; contract grant number: GM079542
Contract grant sponsor: Shriners Hospitals for Children; contract grant number: 84050

cooling was found to reduce the range of pore diameters in scaffolds by increasing the rate of heat transfer due to the increased heat capacity of the liquid compared with air or other system components. Schoof et al.[13] froze CG co-precipitates unidirectionally in a specialized device cooled with liquid nitrogen to yield scaffolds with more homogeneous pore dimensions. O'Brien *et al* regulated the pore size of CG scaffolds by decreasing the freezing rate of the CG co-precipitate as a function of the time of the freezing period from an ambient temperature to a target temperature of $-40^{\circ}C$.[17]

Previous studies from this laboratory have reported the treatment of large full thickness burn injuries with an engineered skin substitutes (ESS) consisting of cultured epidermal keratinocytes and dermal fibroblasts attached onto CG scaffolds. ESS have been shown to close wounds in animal and human studies by morphogenesis and transplantation of skin cells on a degradable CG scaffold, followed by rapid vascularization of the ESS.[6,18–21] ESS provide an epidermal barrier to close the wound, a basement membrane for biological adhesion of epithelial cells to the body, and rapid ingrowth of vascular tissue to perfuse the transplanted tissue substitute.[18,22,23] Kinetic changes in anatomy and physiology of ESS have been determined by histological sampling, determination of surface hydration of the engineered epidermis, and quantitative assessment of metabolic viability.[21,24–26]

In the present study, ESS were prepared with CG scaffolds the homogenate for which was sealed in aluminum casting frames and frozen with liquid nitrogen in a programmable controlled-rate freezer. Hypothetically, regulation of the freezing rate of the polymer homogenate will generate scaffolds with predictable structures, and also deliver a report of technical specifications of each freezing run. Experimental scaffolds were populated with human skin cells and compared with ESS prepared with scaffolds fabricated by immersion of the homogenate-filled casting frames in chilled ethanol as reported in previous studies.[27]

MATERIALS AND METHODS

CG homogenate preparation

Comminuted bovine skin collagen (Kensey Nash; Exton, PA) was powdered with a Wiley Mill (Thomas Scientific; Swedesboro, NJ), dispersed and partially solubilized in 0.5*M* Acetic Acid. The collagen suspension was then co-precipitated by drop-wise addition of chondroitin-6-sulfate (Sigma-Aldrich; St. Louis, MO) in a temperature controlled, refrigerated (4–8°C) tempering beaker. Co-precipitation was performed with high-speed (5300 rpm), high-shear overhead mixing (IKA Works; Staufen, Germany) to homogenize the co-precipitates.[28,29] The resulting CG homogenates were then centrifuged (1800 rpm) to remove excess bubbles, and stored at 4°C before further processing.

CG polymer scaffold formation

CG homogenates were removed from refrigeration and injected into aluminum casting frames [Figure 1(A)].[27,29] Membrane thickness was maintained by a compressible gasket positioned between the two plates of the frames.[28,29] Once the frames were filled, the homogenates were frozen in a pre-chilled 95% ethanol bath ($-55^{\circ}C$), or a programmable, gaseous-phase, liquid nitrogen freezing chamber [Figure 1(A); Custom Biogenics Systems; Romeo, MI]. The chamber of the controlled-rate freezer was custom built to hold four aluminum frames, and programmed by software on an integrated laptop computer. Liquid nitrogen was injected and dispersed with a fan through a grate on the left end of the chamber, and evaporated as it traveled toward the exhaust port on the right end of the freezing chamber. As shown in Figure 1(B), programs (black line) consisted of six steps: (1) Temperature rate from ambient to 4°C; (2) Temperature hold at 4°C; (3) Phase transition rate from 4 to $-90^{\circ}C$ (independent variable); (4) Temperature hold at $-90^{\circ}C$; (5) Temperature rate from -90 to $-60^{\circ}C$ (10°C/min); (6) Temperature hold at $-60^{\circ}C$. Freezing programs were written to cool the chamber from 4 to $-90^{\circ}C$ (Step 3) at rates of -10, -20, -40, and $-80^{\circ}C$/min. Maximum chamber cooling was limited to $-80^{\circ}C$/min because higher rates caused the freezing chamber to flood with liquid nitrogen before it could be dispersed by the fan and vaporize. Other steps in the programs were held constant. A thermocouple probe recorded the homogenate temperature during freezing (green line).

Lyophilization, cross-linking, and storage of scaffolds

After freezing, the casting frames were separated, and the frozen CG sheets (17 cm × 47 cm × 0.15 cm) were transferred as rapidly as possible (i.e., <1 min) to the refrigerated shelves ($-55^{\circ}C$) of a Virtis Ultra 25 EL lyophilizer (Virtis; Gardiner, NY), and lyophilized overnight under constant conditions (30 mTorr, 30°C). The dried CG scaffolds were then processed by dehydrothermal cross-linking at 140°C under vacuum for 24 h. Test scaffolds ($\sim 9 \times 9$ cm^2) were selected for cell culture from three constant locations within the sheets that were proximal, medial and distal to the liquid nitrogen injector. Scaffolds were rehydrated as previously described,[27] and stored in 70% ethanol until use. Just before inoculation of human fibroblasts (hF), scaffolds were rinsed repeatedly with HEPES' Buffered Saline (HBS) followed by incubation UCMC 160 medium.[18,21]

Sampling plan and measurements of pore area and pore fraction

Eight 1.2-cm punches were collected adjacent to the perimeters of each of the six rehydrated scaffolds designated for cell culture (48 samples per condition). Samples were rehydrated in 70% ethanol, processed for histology, embedded in paraffin, sectioned, and stained with aniline blue. Samples were orientated parallel to the inoculation surface, and were sectioned in serial 4 μm increments. Four digital images per sample were collected with a Spot Junior camera on a Nikon FXA photomicroscope at a magnification of 40× to yield a total of 192 images per condition. Each image had an area of 5.2e4 μm^2. Images were processed and analyzed using Photoshop to fill pore areas, and Image J software to quantify pore areas (μm^2). Area values were exported from

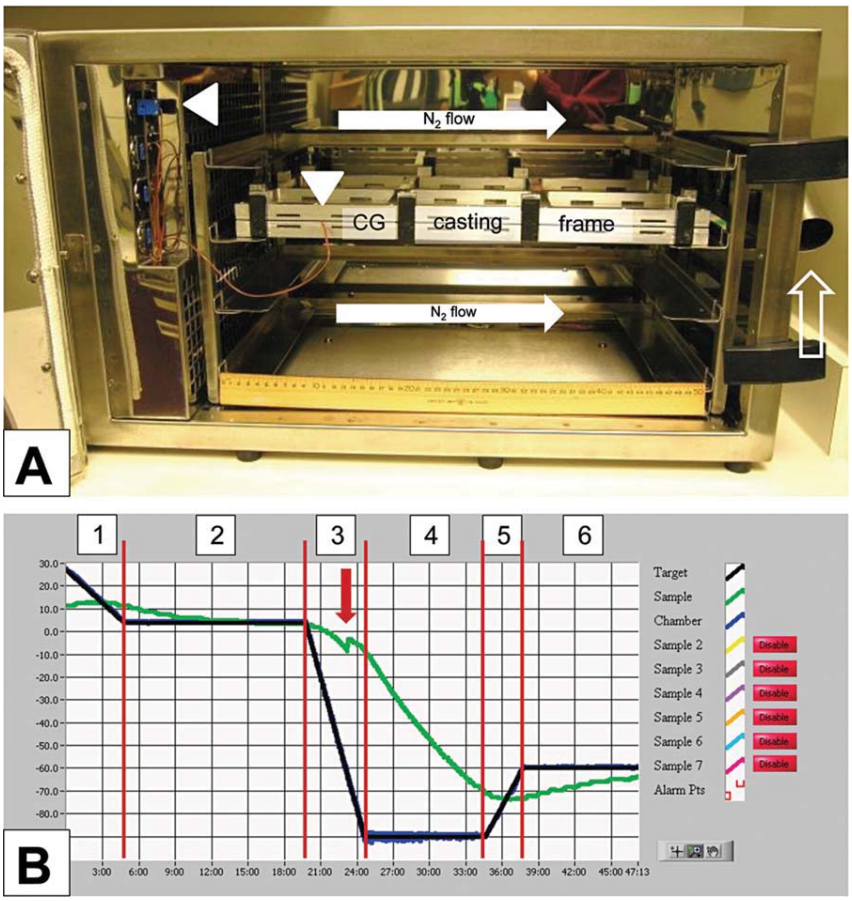

FIGURE 1. Controlled-rate freezing chamber, CG casting frame, and diagram of a representative freezing profile. A) The controlled-rate freezing chamber and CG casting frame. Liquid nitrogen is injected into the chamber and dispersed by a fan from the left end of the chamber through a grate. The liquid evaporates and flows left to right (horizontal arrows) through the chamber flooding all sides of the CG casting frame to remove heat and freeze the CG homogenate before exiting the chamber through the exhaust port (hollow vertical arrow). The temperature of the CG homogenate may be monitored continuously with a thermocouple sensor (white arrowheads) connected to the computer recording system. Scale at bottom of chamber = 50 cm. B) Diagram of the six steps that were used in the experimental freezing program (black line; ordinate axis, temperature; abscissa axis, time in minutes): (1) Ambient temperature to 4°C; (2) Hold at 4°C; (3) Temperature plunge to induce freezing (red arrow, heat of fusion); (4) Hold at −90°C; (5) Temperature ramp to −60°C at 10°C/min; (6) Hold at −60°C. The freezing record from the thermocouple sensor (green line) shows the sample temperature throughout the freezing process. Note that in step 3 of this example, the chamber temperature drops at a rate of −20°C/min, while the sample cools at a rate of −3°C/min as it transitions through the heat of fusion. In step 4, the chamber temperature is held constant at -90°C (0°C/min), while the sample cooling proceeds at approximately −6°C/min to −70°C. After freezing, the top plate of the casting frame is removed, and the bottom plate carrying the frozen CG homogenate is transferred to the pre-chilled shelves of the lyophilizer at −55°C.

Image J to MS Excel for compilation. Data were transferred to SigmaPlot to generate plots.[30] Pore fraction was calculated as: ((total measured pore area per microscopic field / total area per microscopic field) × 100 = % Pore Fraction) from 192 images per condition.

Cell culture

Cultured human fibroblasts (hF) or keratinocytes (hK) were isolated from de-identified surgical discard tissue which was acquired with exemption from informed consent by the Institutional Review Board according to 45CFR46.101(b)(4) of the US Code of Federal Regulations. Primary cultures of hF and hK were cryopreserved, recovered from frozen storage, inoculated into standard tissue culture flasks and allowed to proliferate in selective media as previously described.[19] Fibroblast and keratinocyte populations were inoculated onto CG scaffolds in UCMC 160 medium at densities of 5.0e5/cm^2 and 1.0e6/cm^2 respectively, approximately 24–48 h apart.[19,31] Completed ESS were then incubated at the air/liquid interface on stainless steel supports for 21 days. For the first 3 days, ESS were incubated in UCMC 160 medium. Subsequently, ESS were incubated in UCMC161 medium for the remainder of the culture period.[19] UCMC161 was identical to UCMC160, except that Epidermal Growth Factor and progesterone were removed. Three ESS devices were prepared for each of two experiments (n = 6). One ESS device was lost to contamination from each of the −80°C/min and EtOH control conditions which resulted in n = 5 samples for evaluation in each of those conditions.

Data collection

Histological sampling. Representative samples of each ESS (n = 5–6 per condition) were prepared for histological analysis at incubation day 14.

Surface electrical capacitance (SEC). Surface hydration was measured with a Dermal Phase Meter 9003 (NOVA Technologies; Panama City, FL) on incubation days 6, 8, 14, and 21. Four readings were taken per sample at each time point as previously described.[24,32]

MTT assay. Conversion of 3-(4,5-Dimethylthiazol-2-yl)-2,5-diphenyltetrazolium bromide (MTT) to formazan was measured colorimetrically (OD_{590}) on incubation days 7, 14, and 21 as previously described.[25,30] Four 6-mm punches were taken from a quadrant of each sample at each time point.

Statistical analysis. Data from pore area and pore fraction determinations were analyzed by One-Way Analysis of Variance (ANOVA) followed by pairwise comparisons by Tukey's test. Correlations between variables (r^2) were performed by second order logarithmic regression analysis. Data from SEC and MTT measurements were analyzed by Repeated-Measures ANOVA. Statistical significance was accepted at the 95% confidence level ($p < 0.05$).

RESULTS

A representative freezing record for the CG co-precipitate is shown in Figure 1(B) (green line). The chamber cooling rate in program step 3 (black line) was designed to regulate the rate of freezing through the heat of fusion (red arrow), and subsequently to approximately −70°C in step 4. Importantly, the rapid cooling of the chamber in step 3 (black line) ranged from 0 to −90°C in about 4.5 min (−20°C/min) while simultaneously the sample cooled from 4 to −10°C (−3°C/min), and transitioned through the heat of fusion. Subsequently in program step 4, the chamber temperature was held constant at −90°C (0°C/min), while simultaneously the polymer was cooled from −10 to −70°C in about 10 min (−6°C/min). Microscopic preparations of acellular CG scaffolds and of ESS collected on incubation day 14 are shown in Figure 2. This time point had the most variability among the conditions with respect to the morphogenesis and organization of the dermal and epidermal compartments of the ESS. CG scaffolds frozen at −10°C/min [Figure 2(A,B)] had the largest and most heterogeneous pore distribution of all of the test conditions. Qualitatively, pore area and pore fraction appear to decrease inversely as a function of the rate of freezing [Figure 2(A,C,E,G)] with similar apparent pore area between a cooling rate of −80°C/min [Figure 2(G)] and the EtOH control [Figure 2(I)]. Controlled-rate freezing (CRF) rates of −10 and −20°C/min exhibited epithelial inclusions [Figure 2(B,D)] within the fibroblast layer of the dermal substitutes (white arrows). Epithelial inclusions indicate a migratory hK phenotype that often leads to formation of 'cysts' within the scaffold after transplantation that may protract epithelial wound closure. The inclusions became less frequent as the pore area decreased as observed in the −40°C/min, −80°C/min, or EtOH conditions. However, all conditions developed a stratified and differentiated epithelium by incubation day 14.

Figure 3(A) shows the measured pore area as a function of freezing rate. The pore area decreased inversely to the rate of chamber cooling during program step 3 (r^2 = 0.96). Variability of pore areas within CG scaffolds also decreased as the rate of freezing increased, ranging (mean ± SEM) from 1470 ± 56.4 for −10°C/min, to 1026 ± 27.2 for −20°C/min, to 511 ± 13.3 for −40°C/min, and to 588 ± 15.0 for −80°C/min. Values for pore area of CG scaffolds frozen in EtOH were 432 ± 12.7. The CRF conditions demonstrated an approximate threefold difference in pore area across the range of freezing rates from −10 to −40°C/min. Figure 3(B) shows the calculated pore fraction of CG scaffolds as a function of freezing rate. The pore fraction decreased inversely to the rate of chamber cooling (r^2 = 0.24). Values for percentage pore fraction ranged (mean ± SEM) from 63.9 ± 0.80% for −10°C/min, to 60.7 ± 0.54% for −20°C/min, to 50.2 ± 0.72% for −40°C/min, and to 51.4 ± 0.70% for −80°C/min. These values showed an approximate 13% difference across the range of chamber cooling rates from −10 to −80°C/min. In contrast to values of pore area, variability (SEM) of pore fractions among CG scaffolds remained relatively constant as the rate of cooling increased. Values for pore fraction of CG scaffolds frozen in EtOH were 48.2 ± 0.97%.

Surface hydration of ESS versus incubation interval is shown in Figure 4. Surface hydration values (DPM Units) decreased approximately fourfold during the incubation period, and corresponded with the development of a keratinized epithelium in the ESS samples. The reference line represents the skin surface hydration of the volar forearms of healthy human volunteers. Surface hydration was similar in all groups, and exhibited a decrease between culture days 6 and 14. DPM values of ESS with scaffolds frozen at −80°C/min were significantly different from those of scaffolds frozen −10°C/min and EtOH control scaffolds at culture day 6. Test groups were not significantly different from the control or each other at culture days 14 and 21, and approached hydration levels of skin barrier in healthy volunteers by incubation day 14. However, each test group was significantly lower at incubation day 14 than readings taken at culture day 6 ($p < 0.05$) indicating epithelial keratinization. Data collected on day 21 remained significantly lower than day 6, but not than incubation day 14. This indicates that developing epidermal barrier remained stable until incubation day 21. CG scaffolds frozen at −10°C/min exhibited an increase in SEC values between days 14 and 21, but this increase was not statistically significant.

Results of the MTT assay are shown in Figure 5. All groups exhibited an increase in optical density values over the culture period. As previously observed, the greatest increase in ODs occurred between incubation days 7 and 14, after which less change was observed between incubation days 14 and 21. Test scaffolds frozen at −10, −40, and

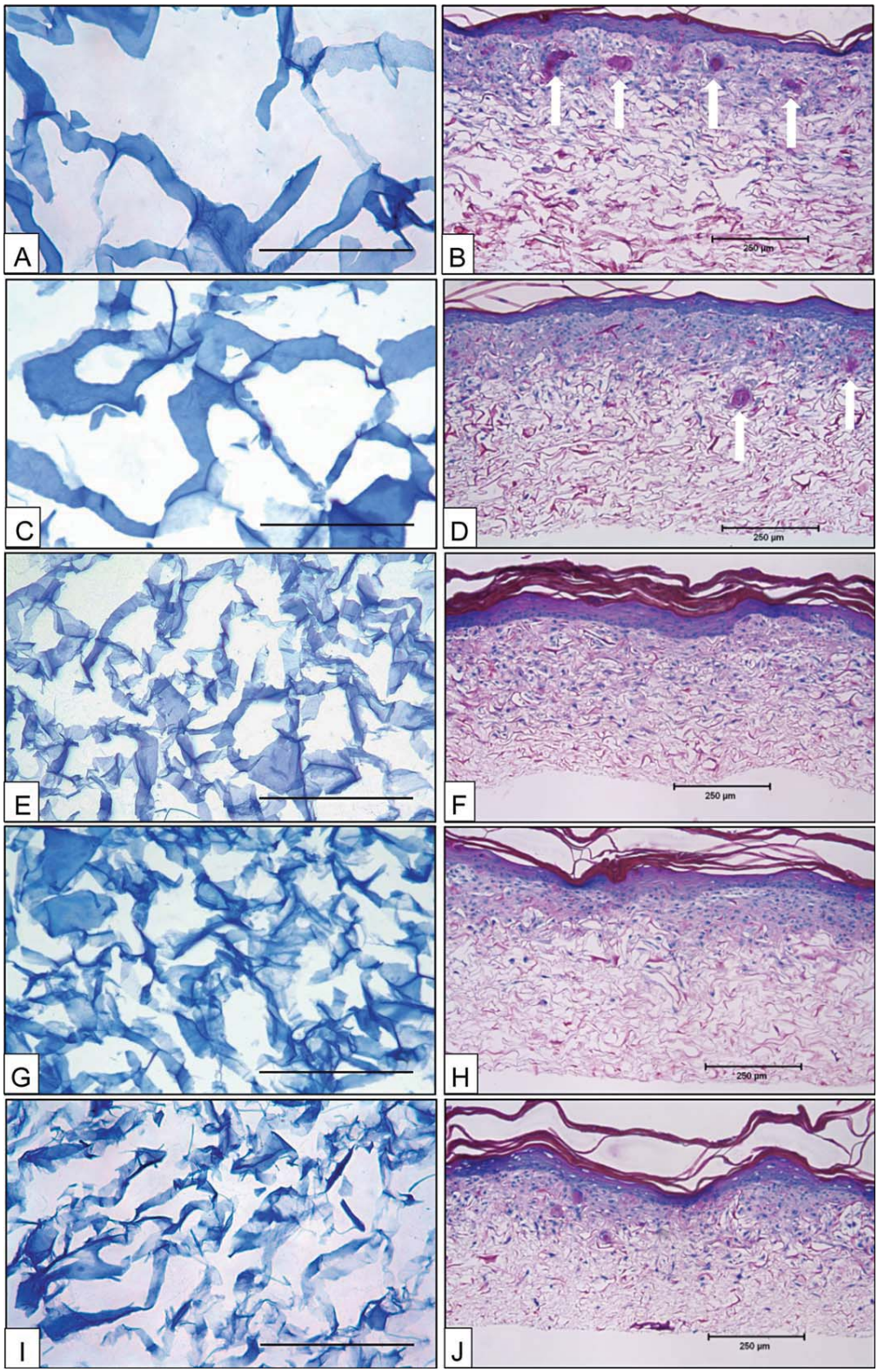

FIGURE 2. Histologies of acellular CG scaffolds and engineered skin substitutes (ESS) at incubation day 14. Scaffolds were prepared by controlled-rate freezing with liquid nitrogen at −10°C/min (A,B), −20°C/min (C,D), −40°C/min (E,F), −80°C/min (G,H), or by submersion in 95% EtOH at −55°C (I,J). Qualitative images of surface histology of acellular scaffolds (A, C, E, G, I) demonstrates the decrease of pore area and pore fraction as an inverse function of freezing rate. Scale bars = 50 µm. Cross-sections of the ESS samples (B, D, F, H, J) shows development of keratinized layers, but epithelial morphogenesis the in the −40°C/min (C) and −80°C/min (D) conditions was most similar to the EtOH control. Scale bars = 0.25 mm.

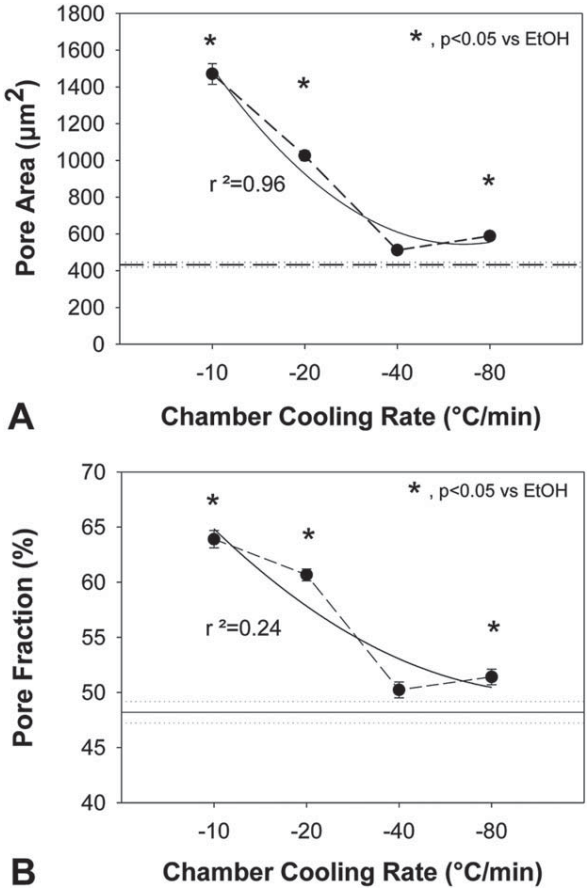

FIGURE 3. Plots of chamber cooling rates versus pore area and pore fraction. A) Second order regression (solid line) shows a significant inverse correlation (r^2 = 0.96) between chamber cooling rates in the controlled-rate freezer, and pore area of hydrated CG scaffolds in the range of −10 to −80°C/min. The horizontal reference lines are the mean pore area (±SEM) of scaffolds prepared by freezing in a 95% EtOH bath at −55°C. All CRF conditions, except −40°C/min, were different from the EtOH control. B) Second order regression (solid line) shows a significant inverse correlation (r^2 = 0.24) between chamber cooling rates and pore fraction of hydrated CG scaffolds in the range of −10 to −80°C/min. The horizontal reference lines are the mean pore fractions (±SEM) of scaffolds prepared by freezing in a 95% EtOH bath at −55°C. All CRF conditions, except for −40°C/min, were different from the EtOH control.

−80°C/min were significantly different between culture days 7 and 14. MTT values were significantly different at culture day 7 between scaffolds frozen at −10°C/min compared with scaffolds frozen at either −20 or −80°C/min. Scaffolds frozen at −40°C/min were also different from scaffolds frozen at −80°C/min. MTT values at culture day 14 for ESS prepared from scaffolds frozen at −80°C/min differed significantly from the EtOH control, but not from other conditions. Finally, at culture day 21 scaffolds frozen at −80°C/min were different from all other test groups and control scaffolds.

DISCUSSION

The use of a programmable, liquid nitrogen-cooled, controlled-rate freezer was effective at freezing CG co-precipitates with an optimal pore area to allow cell attachment, survival, and morphogenesis of an engineered skin substitute. CG scaffolds fabricated with a controlled-rate freezer exhibited similar physical and handling to scaffolds fabricated with a pre-chilled ethanol bath *in vitro*. However, the controlled-rate freezer eliminated the use of flammable liquids in the fabrication process, increased the precision and accuracy of the cooling process, and generated a continuous record of the freezing process from initiation to completion.

The isotropic removal of heat from all sides of the metallic casting frame simultaneously results from flooding or submerging in chilled fluids (95% EtOH or N_2) and generates scaffolds with symmetric pore distributions across their thicknesses. By comparison, freezing of aqueous polymers in a metal pan on the shelf of a lyophilizer has a much higher heat conductivity and freezing rate on the "pan side" than on the "air side"[11,33] which is insulated, and tends to generate scaffolds with smaller pores on the "pan side", progressing to larger pores on the "air side". Although the preferred distribution pores in the scaffold depends on the intended application, the purpose of this study was to generate scaffolds with symmetric and uniform pore distribution to promote both mechanical strength and cellular migration and proliferation. Therefore, the isotropic removal of heat with chilled fluids provides greater uniformity of scaffold structure than anisotropic heat removal through a metal pan on a refrigerated shelf of a lyophilizer.

Experimental data supports the use of a controlled-rate freezer to effectively regulate the pore area, pore fraction, and structural uniformity of CG scaffolds. As reported elsewhere, increasing the freezing rate during phase transition, decreased the size of ice crystals resulting in smaller pores in the freeze-dried scaffolds.[11,12,14,17] In the current study, the rate of chamber cooling during the phase transition of the polymer was increased incrementally to regulate the freezing rate, and other steps in the computer-controlled freezing program were held constant [Figure 1(B)]. Other factors that have been shown to influence pore size, such as acid concentration, homogenate volume, total time of freezing,[12] cross-linking agents,[30] starting material source and concentration[8,21] were also held constant. Another factor that may regulate the ice structure before freeze-drying is the time of transfer from the freezing chamber to the lyophilizer. Because the freezing processes described here were performed outside of the lyophilizer, the time of transfer was held to a minimum (<1 min) between the freezing chambers at approximately −60°C, and the lyophilizer shelf at −55°C. In addition, because the casting frame is a closed vessel, it must be opened, and the aluminum plates separated to transfer the frozen polymer to the lyophilizer. This procedure typically requires 30–60 s, but the polymer is exposed to ambient temperature for only a fraction of that time due to its location between two aluminum plates. Because of these provisions, heat gain by the polymer during the transition from the freezing chamber to the lyophilizer is considered to be negligible.

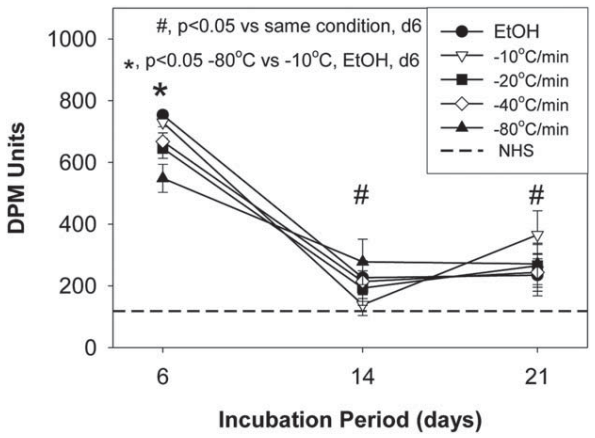

FIGURE 4. Plot of Dermal Phase Meter (DPM) units versus incubation period. Hydration of the epithelial surface of ESS (DPM units) decreased for all conditions between incubation days 6 and 14, indicating development of a keratinized surface. The DPM values for the −80°C/min CRF condition were statistically lower than the −10°C/min and EtOH control at day 6 (*, $p < 0.05$). From day 14 to day 21, CRF conditions −10 and −20°C/min, increased indicating deterioration of the keratinized layer. Other conditions remained stable between 14–21 days of incubation. Skin surface hydration of healthy volunteers is shown in the reference (dashed) line.

The differences in pore area were evident in histological images of CG scaffolds in ESS prepared on culture day 14 (Figure 2). As hypothesized, CG scaffolds frozen at −10°C/min had the largest and greatest variability of pore area. These scaffolds also exhibited irregular distributions of dermal fibroblasts. This heterogeneity in the dermal component led to a heterogeneity in organization of the epidermal component of the engineered skin as represented by the formation of epithelial inclusions [Figure 2(B,D), white arrows)]. Formation of epithelial inclusions *in vitro* results, in part, from insufficient contact with fibroblasts, and a migratory phenotype that can contribute to formation of epithelial cysts after transplantation. Epithelial cysts, in turn, may protract maturation of the transplanted epithelium, or if extensive, may contribute to graft failure. Poor epidermal organization suggests heterogeneous contact between fibroblasts and keratinocytes, which are known to spontaneously form basement membrane if in direct contact.[18] Compartmentalization of the dermal and epidermal components had developed by culture day 14 in the −10°C/min condition. However, there was a greater degree of epithelial invasion of the scaffold than in other conditions.

In the −40°C/min and −80°c/min test groups, there were higher degrees of organization at incubation day 14, than at day 7 (not shown). In most samples from each condition, the three essential components of ESS morphology were found; the CG scaffolds, uniformly-distributed layers of dermal fibroblasts, and epidermal keratinocytes that formed a stratified epidermal component. Importantly, the epidermal component contained a basal cell layer in contact with hF, nucleated suprabasal keratinocytes analogous to a spinous layer, a granular layer, and keratinized layers. The basal cells are the most proliferative, and retention of this population promotes permanent closure of treated wounds.[18,19,34,35] Development of a highly proliferative basal keratinocyte layer depends on formation of basement membrane which depends on direct contact between continuous layers of fibroblasts and keratinocytes.

The keratinized epithelium provides a physical barrier between the wound bed and the environment, and initiates formation of the protective *stratum corneum*. Development of the keratinized layer is also important in reducing the risk of infection and fluid loss after the ESS is grafted to the wound. Development of this layer appeared to coincide with an increase in freezing rate, as noted in histological samples at culture day 14 (Figure 2), and in surface hydration data (Figure 4). If so, epidermal barrier was likely to have resulted indirectly from improved attachment and survival of the hF population after inoculation, and to a more uniform cellular surface on which keratinocytes attached and formed basement membrane. The differences in pore area did not affect negatively the measured surface hydration (Figure 4), which serves as a surrogate measure of epithelial keratinization and epidermal barrier.[24,36,37] All groups exhibited a significant reduction in surface hydration values over time. This decrease over time indicated that cellular morphogenesis and maturation took place normally. The increase in surface hydration values of ESS with scaffolds frozen at −10°C/min suggests premature degeneration between incubation days 14–21, as observed in histological samples at incubation day 21 (not shown). The absence of nucleated keratinocytes in the basal layer at the dermal/epidermal junction confirmed that most cells in the −10°C/min condition had terminally differentiated, and had lost their abilities to proliferate and provide stable, long-term wound closure.

CRF did not seem to have a detrimental impact on cellular viability as measured in the MTT assay. If test conditions were compared among each other, there was a general trend of increasing MTT values at culture day 14 with increasing freezing rates. MTT values of ESS with scaffolds

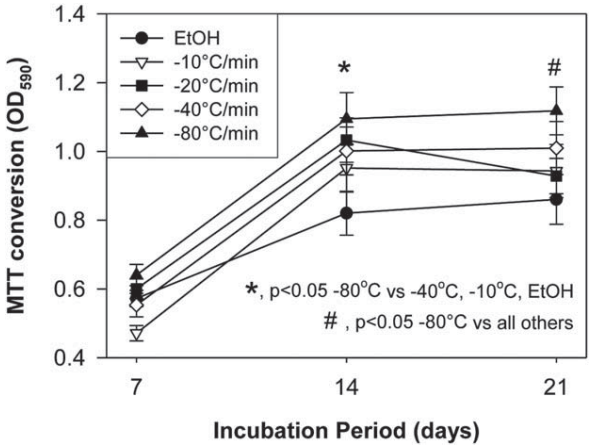

FIGURE 5. Plot of MTT conversion (OD_{590}) versus incubation period. All CRF conditions showed quantitatively higher cell viability than the EtOH control by MTT conversion at incubation days 14 and 21. MTT of ESS with scaffolds frozen at −80°C was significantly different from the EtOH control at incubation day 14, and from all other conditions at incubation day 21.

frozen at −80°C/min were significantly higher than ESS with scaffolds frozen at −10°C/min, −40°C/min, or controls. This trend was consistent with histological samples at corresponding time points. Cellular viability and graft anatomy appeared to improve with increasing freezing rates, but it is not possible to attribute MTT values to either of the cell types in the ESS. All ESS fabricated with scaffolds prepared by CRF had higher MTT values than ESS with scaffolds made by freezing in chilled ethanol. Together with histology and quantitative analysis of surface hydration, MTT provides a measure of mitochondrial metabolism that can serve as a criterion for quality assurance of ESS.[18,38] Although the structural composition of the scaffolds was modified in this study, selected factors, such as fluid permeability, degradation rate and mechanical properties.[32,39,40] were not evaluated here. However, because these factors may be affected by structural changes in the scaffolds, they deserve further analyses in future studies, together with transplantation for evaluations of wound closure.

Part of the novelty of this study derives from the use of chilled fluids as a gas or a liquid for indirect freezing of CG homogenates. Gaseous fluid (i.e., evaporated liquid N_2) replaces liquid fluid (95% EtOH) used previously as the coolant for freezing of the homogenates. Heat removal is effective for both methods, but the use of evaporated liquid N_2 as the coolant simplifies the freezing step, eliminates the use of flammable liquids in the fabrication process, and uses a computer-controlled program that generates an operational report and electronic record. The implementation of a digital control system in the freezing process improves both the accuracy and reproducibility of scaffold fabrication. Conversely, liquid EtOH has far greater heat capacity than evaporated liquid N_2, and provides greater uniformity of heat transfer at a higher temperature, but it is difficult to contain and uses an analog process that requires manual records. Overall, the advantages of the CRF process outweigh those of liquid cooling in EtOH, and are more conducive for manufacturing of medical products.

In conclusion, use of liquid nitrogen as a coolant in a programmable, controlled-rate freezer was effective in producing CG scaffolds with structural and biochemical characteristics similar to CG scaffolds frozen in a pre-chilled bath of 95% EtOH. Pore areas were clearly controllable and correlated well with the freezing rates, a finding which is consistent with the physical principles of ice crystallization. Variation within each lyophilized sheet decreased as the freezing rate increased. Cellular attachment, viability, and morphogenesis were comparable among ESS prepared with CG scaffolds fabricated by CRF at −40°C\min, −80°C\min, or submersion in chilled EtOH. The precision and convenience of the CRF process offer multiple advantages for fabrication of lyophilized biopolymer scaffolds for applications in tissue engineering and regenerative medicine.

ACKNOWLEDGMENTS

The authors thank Deanna Leslie for histology, Rachel Zimmerman and William Kossenjans for preparation of nutrient media, and Laura James for statistical analyses.

REFERENCES

1. Abou Neel EA, Bozec L, Knowles JC, Syed O, Mudera V, Day R, Hyun JK. Collagen: Emerging collagen-based therapies hit the patient. Adv Drug Deliv Rev 2013;65:429–456.
2. Ferreira AM, Gentile P, Chiono V, Ciardelli G. Collagen for bone tissue regeneration. Acta Biomater 2012;8:3191–3200.
3. Galler KM, D'Souza RN, Hartgerink JD, Schmalz G. Scaffolds for dental pulp tissue engineering. Adv Dent Res 2011;23:333–339.
4. Yannas IV, Tzeranis DS, Harley BA, So PT. Biologically active collagen-based scaffolds: Advances in processing and characterization. Philos Transact A Math Phys Eng Sci 2010;368:2123–2139.
5. Badylak SF, Freytes DO, Gilbert TW. Extracellular matrix as a biological scaffold material: Structure and function. Acta Biomater 2009;5:1–13.
6. Boyce ST, Warden GD. Principles and practices for treatment of cutaneous wounds with cultured skin substitutes. Am J Surg 2002;183:445–456.
7. Smith IO, Liu XH, Smith LA, Ma PX. Nanostructured polymer scaffolds for tissue engineering and regenerative medicine. Wiley Interdiscip Rev Nanomed Nanobiotechnol 2009;1:226–236.
8. Willard JJ, Drexler JW, Das A, Roy S, Shilo S, Shoseyov O, Powell HM. Plant-derived human collagen scaffolds for skin tissue engineering. Tissue Eng Part A 2013;19:1507–1518.
9. Matthews JA, Wnek GE, Simpson DG, Bowlin GL. Electrospinning of collagen nanofibers. Biomacromolecules 2002;3:232–238.
10. Yannas IV, Burke JF. Design of an artificial skin. I Basic design principles. J Biomed Mater Res 1980;14:65–81.
11. Boyce ST, Christianson DJ, Hansbrough JF. Structure of a collagen-GAG dermal skin substitute optimized for cultured human epidermal keratinocytes. J Biomed Mater Res 1988;22: 939–957.
12. Schoof H, Apel J, Heschel I, Rau G. Control of pore structure and size in freeze-dried collagen sponges. J Biomed Mater Res 2001; 58:352–357.
13. Schoof H, Bruns L, Heschel I, Rau G. Dendritic ice morphology in unidirectionally solidified collagen suspensions. J Crystal Growth 2000;209:122–129.
14. Dagalakis N, Flink J, Stasikelis P, Burke JF, Yannas IV. Design of an artificial skin. III. Control of pore structure. J Biomed Mater Res 1980;14:511–528.
15. Taylor MJ, Baicu S. Review of vitreous islet cryopreservation: Some practical issues and their resolution. Organogenesis 2009;5: 155–166.
16. Wen F, Magalhaes R, Gouk SS, Bhakta G, Lee KH, Hutmacher DW, Kuleshova LL. Vitreous cryopreservation of nanofibrous tissue-engineered constructs generated using mesenchymal stromal cells. Tissue Eng Part C Methods 2009;15:105–114.
17. O'Brien FJ, Harley BA, Yannas IV, Gibson LJ. The effect of pore size on cell adhesion in collagen-GAG scaffolds. Biomaterials 2005;26:433–441.
18. Boyce ST, Supp AP, Swope VB, Warden GD. Vitamin C regulates keratinocyte viability, epidermal barrier, and basement membrane in vitro, and reduces wound contraction after grafting of cultured skin substitutes. J Invest Dermatol 2002;118:565–572.
19. Boyce ST, Rice RK, Lynch KA, Supp AP, Swope VB, Kagan RJ, Supp DM. Assessment of replication rates of human keratinocytes in engineered skin substitutes grafted to athymic mice. Wound Repair Regen 2012;20:544–551.
20. Boyce ST, Kagan RJ, Meyer NA, Yakuboff KP, Warden GD. *The 1999 Clinical Research Award*. Cultured skin substitutes combined with Integra to replace native skin autograft and allograft for closure of full-thickness burns. J Burn Care Rehabil 1999;20:453–461.
21. Boyce ST, Kagan RJ, Greenhalgh DG, Warner P, Yakuboff KP, Palmieri T, Warden GD. Cultured skin substitutes reduce requirements for harvesting of skin autograft for closure of excised, full-thickness burns. J Trauma 2006;60:821–829.
22. Supp DM, Supp AP, Bell SM, Boyce ST. Enhanced vascularization of cultured skin substitutes genetically modified to overexpress vascular endothelial growth factor. J Invest Dermatol 2000;114:5–13.
23. Supp DM, Wilson-Landy K, Boyce ST. Human dermal microvascular endothelial cells form vascular analogs in cultured skin substitutes after grafting to athymic mice. FASEB J 2002;16:797–804.

24. Boyce ST, Supp AP, Harriger MD, Pickens WL, Wickett RR, Hoath SB. Surface electrical capacitance as a noninvasive index of epidermal barrier in cultured skin substitutes in athymic mice. J Invest Dermatol 1996;107:82–87.
25. Swope VB, Supp AP, Greenhalgh DG, Warden GD, Boyce ST. Expression of insulin-like growth factor-I by cultured skin substitutes does not replace the physiologic requirement for insulin *in vitro*. J Invest Dermatol 2001;116:650–657.
26. Vicanova J, Boyce ST, Harriger MD, Weerheim A, Bouwstra J, Ponec M. Stratum corneum lipid composition and structure in cultured skin substitutes is restored to normal after grafting onto athymic mice. J Invest Dermatol 1998;3:114–120.
27. Boyce ST. Methods for the serum-free culture of keratinocytes and transplantation of collagen-GAG-based skin substitutes. In: Morgan JR, Yarmush ML, editors. Methods in Molecular Medicine, Vol. 18: Tissue Engineering Methods and Protocols. Totowa, NJ: Humana Press Inc.; 1999. pp 365–389.
28. Boyce ST. Apparatus for preparing a biocompatible matrix. United States Patent #6,905,105; 2005.
29. Boyce ST. Apparatus for preparing a biocompatible matrix. United States Patent #7,452,720; 2008.
30. Powell HM, Boyce ST. EDC cross-linking improves skin substitute strength and stability. Biomaterials 2006;27:5821–5827.
31. Swope VB, Supp AP, Schwemberger S, Babcock GF, Boyce ST. Increased expression of integrins and decreased apoptosis correlate with increased melanocyte retention in cultured skin substitutes. Pigment Cell Res 2006;19:424–433.
32. Goretsky MJ, Supp AP, Greenhalgh DG, Warden GD, Boyce ST. *The 1995 Young Investigator Award*: Surface electrical capacitance as an index of epidermal barrier properties of composite skin substitutes and skin autografts. Wound Rep Reg 1995;3:419–425.
33. O'Brien FJ, Harley BA, Yannas IV, Gibson L. Influence of freezing rate on pore structure in freeze-dried collagen-GAG scaffolds. Biomaterials 2004;25:1077–1086.
34. Jensen UB, Lowell S, Watt FM. The spatial relationship between stem cells and their progeny in the basal layer of human epidermis: A new view based on whole-mount labeling and lineage analysis. Development 1999;126:2409–2418.
35. Barai ND, Supp AP, Kasting GB, Visscher MO, Boyce ST. Improvement of epidermal barrier properties in cultured skin substitutes after grafting onto athymic mice. Skin Pharmacol Physiol 2006;20:21–28.
36. Treffel P, Gabard B. Stratum corneum dynamic function measurements after moisturizer or irritant application. Arch Dermatol Res 1995;287:474–479.
37. Okah FA, Wickett RR, Pickens WL, Hoath SB. Surface electrical capacitance as a noninvasive bedside measure of epidermal barrier maturation in the newborn infant. Pediatrics 1995;96:688–692.
38. Powell HM, Boyce ST. Fiber density of electrospun gelatin scaffolds regulates morphogenesis of dermal-epidermal skin substitutes. J Biomed Mater Res A 2007;84:1078–1086.
39. Parenteau-Bareil R, Gauvin R, Cliche S, Gariepy C, Germain L, Berthod F. Comparative study of bovine, porcine and avian collagens for the production of a tissue engineered dermis. Acta Biomater 2011;7:3757–3765.
40. Kanungo BP, Gibson LJ. Density-property relationships in collagen-glycosaminoglycan scaffolds. Acta Biomater 2010;6:344–353.